



## Electronic density of states and metastability of icosahedral Au–Al–Yb quasicrystal



S. Jazbec<sup>a</sup>, S. Vrtnik<sup>a</sup>, Z. Jagličič<sup>b</sup>, S. Kashimoto<sup>c</sup>, J. Ivkov<sup>d</sup>, P. Popčević<sup>d</sup>, A. Smontara<sup>d</sup>, Hae Jin Kim<sup>e</sup>, Jin Gyu Kim<sup>e</sup>, J. Dolinšek<sup>a,f,\*</sup>

<sup>a</sup> J. Stefan Institute & University of Ljubljana, Faculty of Mathematics and Physics, Jamova 39, SI-1000 Ljubljana, Slovenia

<sup>b</sup> Institute of Mathematics, Physics and Mechanics & University of Ljubljana, Faculty of Civil and Geodetic Engineering, Jadranska 19, SI-1000 Ljubljana, Slovenia

<sup>c</sup> Division of Applied Physics, Hokkaido University, Kita-ku, 060-8628 Sapporo, Japan

<sup>d</sup> Institute of Physics, Bijenička 46, POB 304, HR-10001 Zagreb, Croatia

<sup>e</sup> Division of Materials Science & Division of Electron Microscopy, Korea Basic Science Institute, Daejeon 305-333, Republic of Korea

<sup>f</sup> EN-FIST Centre of Excellence, Dunajska 156, SI-1000 Ljubljana, Slovenia

### ARTICLE INFO

#### Article history:

Received 22 August 2013

Received in revised form 10 October 2013

Accepted 10 October 2013

Available online 19 October 2013

#### Keywords:

Quasicrystals

Electronic properties

Electrical transport

### ABSTRACT

The recently discovered icosahedral quasicrystal (*i*-QC) in the ternary Au–Al–Yb system at the composition Au<sub>51</sub>Al<sub>34</sub>Yb<sub>15</sub> is formed only in as-cast alloys and is metastable with decomposition to other crystalline phases upon annealing at 700 °C. Measuring the electronic transport coefficients (electrical resistivity, thermoelectric power, Hall coefficient), magnetic susceptibility and specific heat, we addressed the question of metastability of the *i*-Au–Al–Yb quasicrystalline phase by reconstructing the shape of the electronic density of states (DOS) in the vicinity of Fermi level  $\varepsilon_F$  with the aim to find out whether there exists a pseudogap in the DOS that could contribute to electronic stabilization of the icosahedral phase. The results have revealed that the DOS in the vicinity of  $\varepsilon_F$  exhibits a pronounced valley on a 100 meV energy scale with a sharp feature on a 10 meV scale, both being centered almost exactly at  $\varepsilon_F$ . This pseudogap is apparently not wide enough to ensure sufficient electronic energy gain of the order of a few 10 kJ/mol needed for the electronic stabilization of the icosahedral phase. A possible origin of metastability of the *i*-Au–Al–Yb quasicrystal and thermodynamic stability of its 1/1 cubic approximant of very similar composition is discussed. The sharp feature in the DOS at  $\varepsilon_F$  is proposed to originate from indirect interaction between localized Yb *f*-moments due to overlap of their polarization clouds in the presence of hybridization of the *f* and *s* states, which leads to a sharp resonance peak.

© 2013 Elsevier B.V. All rights reserved.

### 1. Introduction

Recently, an icosahedral quasicrystal (*i*-QC) was discovered in the ternary Au–Al–Yb system at the composition Au<sub>51</sub>Al<sub>34</sub>Yb<sub>15</sub> [1]. The quasicrystal is formed only in as-cast alloys and is regarded as metastable with decomposition to other crystalline phases upon annealing at 700 °C. The predominant phase in the annealed specimen is a 1/1 cubic approximant, which is stable at the composition Au<sub>51</sub>Al<sub>35</sub>Yb<sub>14</sub> at 700 °C. The *i*-Au<sub>51</sub>Al<sub>34</sub>Yb<sub>15</sub> QC is isostructural to the binary icosahedral *i*-Cd<sub>5,7</sub>Yb [2–4], which is considered as a prototype structure of the group of Tsai-type *i*-QCs. The *i*-Cd<sub>5,7</sub>Yb-type structure is realized in many alloy systems by replacing the majority element cadmium with Zn, Zn–M (M = Mg, Cu, Pd, Ag, Pt, Au), Zn–T (T = Mn, Fe, Co, Ni), Cu–Al, Cu–Ga, Cd–Mg, Ag–Al, Ag–In,

Pd–Al, Au–Ga and Au–In, whereas the minor component can be trivalent transition elements such as Sc, Y or lanthanides, or divalent Ca or Yb [5,6,1]. In all cases, composition of the minor component ranges from 12 to 16 at.%, and the Tsai-type QCs satisfy an almost constant valence electron concentration per atom *e/a*, ranging from 2.00 to 2.15. This is the first condition of the Hume-Rothery rules [7]. According to the magnitude of the six-dimensional lattice parameter  $a_{6D}$ , the *i*-Au<sub>51</sub>Al<sub>34</sub>Yb<sub>15</sub> QC is situated between the Zn–Sc group with smaller  $a_{6D}$  and the Cd–Yb group with larger values. For the first group, the minor component is always Sc, whereas for the second group it is a larger element such as Ca, Y or lanthanides. Such a combination may be due to the geometrical conditions for the construction of Tsai-type icosahedral atomic clusters, and induces the second condition of the Hume-Rothery rules – the size factor. The two conditions of *e/a* and size factor can be regarded as a substitution rule in Tsai-type QCs.

In view of thermodynamic stability of the prototype *i*-Cd<sub>5,7</sub>Yb structure, metastability of the isostructural *i*-Au–Al–Yb QC deserves further attention. Structure determination of the periodic

\* Corresponding author at: J. Stefan Institute & University of Ljubljana, Faculty of Mathematics and Physics, Jamova 39, SI-1000 Ljubljana, Slovenia. Tel.: +386 1 4773 740; fax: +386 1 4773 191.

E-mail address: [jani.dolinsek@ijs.si](mailto:jani.dolinsek@ijs.si) (J. Dolinšek).

$\text{Au}_{51}\text{Al}_{35}\text{Yb}_{14}$  1/1 cubic approximant phase has revealed that the unit cell contains disorder, where the Al site denoted as M8 (using the nomenclature of Ref. [1]) and the Au–Al sites M1–M7 show both mixed and partial occupancies. Due to structural similarity between the QC and its approximant, it is expected that disorder (both chemical and geometrical) is present in the *i*-Au–Al–Yb QC, too. Metastability at low temperatures of QCs as well as crystalline compounds with inherent quenched disorder is not surprising since the disorder leads to finite configurational entropy in violation of the third law of thermodynamics. A structurally disordered phase can exist in the  $T \rightarrow 0$  limit only as a quenched metastable high-temperature state whose ergodicity is broken on the experimental time scale. According to these considerations one can expect that the *i*-Au–Al–Yb quasicrystalline phase with quenched disorder is metastable at low temperatures, but could exist as an entropically stabilized thermodynamically stable phase at high temperatures. This is in contrast to the experiments, which revealed that the quasicrystal is metastable also at high temperatures.

Apart from the entropic stabilization that is important at high temperatures, quasicrystalline and giant-unit-cell complex intermetallic phases are frequently stabilized electronically by forming a pseudogap in the electronic density of states (DOS) across the Fermi level  $\varepsilon_F$ . The creation of a pseudogap at  $\varepsilon_F$  leads to an efficient lowering of the electronic kinetic energy, which increases the cohesive energy and consequently the stability of the structure [7]. In QCs, a pseudogap close to  $\varepsilon_F$  was frequently found both experimentally and theoretically, with its depth being generally about 20–80% of the free-electron DOS and the width in the range  $\Delta\varepsilon = 1\text{--}2$  eV [8]. In this paper we address the question of stability of the *i*-Au–Al–Yb QC phase by presenting an experimental study of the electronic DOS in the vicinity of  $\varepsilon_F$  with the aim to find out whether the pseudogap is present in this phase. From the temperature-dependent thermoelectric power, the electrical resistivity and the Hall coefficient we reconstruct the shape of the DOS in the near vicinity of  $\varepsilon_F$  and discuss its role in the metastability of the *i*-Au–Al–Yb quasicrystal.

## 2. Sample description and characterization

Our *i*-Au–Al–Yb as-cast polygrain sample with the nominal composition  $\text{Au}_{49}\text{Al}_{34}\text{Yb}_{17}$  was prepared from high purity materials (Alfa Aesar) of Au (foil, 0.5 mm, 99.95%), Al (wire, 1.0 mm diam., 99.999%) and Yb (ingot, 99.95%) using an arc furnace in an Ar atmosphere. Its actual composition was determined by energy dispersive X-ray spectrometry (EDS) to be  $\text{Au}_{51}\text{Al}_{34}\text{Yb}_{15}$  and its powder X-ray diffraction spectrum (not shown) matched the one reported in [1]. Instead of giving further details of the sample characterization by X-ray and microscopy techniques, we present physical properties of our sample (the electrical resistivity, the magnetic susceptibility and the specific heat) as a means of material characterization and demonstrate that these are within the experimental uncertainty the same as those reported for the *i*-Au–Al–Yb samples used by Watanuki et al. [9] and Deguchi et al. [10] in the studies of intermediate-valence character and quantum critical state, respectively, of the *i*-Au–Al–Yb quasicrystal. This equivalence has led us to conclude that structural quality of our *i*-Au–Al–Yb sample was not significantly different from the samples used in other studies [9,10]. Electrical and thermal measurements were conducted by a Quantum Design Physical Property Measurement System PPMS 9T (except the Hall coefficient, which was measured by a laboratory-made apparatus equipped with a 10 kOe electromagnet), whereas magnetic measurements were conducted by a Quantum Design MPMS XL-5 SQUID magnetometer equipped with a 50 kOe magnet.

The electrical resistivity  $\rho(T)$  of our *i*-Au–Al–Yb sample, measured in the temperature range 2–380 K by a standard four-terminal technique, is presented in Fig. 1.  $\rho(T)$  shows positive temperature coefficient with a large residual resistivity  $\rho_{2\text{K}} = 198 \mu\Omega \text{ cm}$  and a relative increase up to room temperature (RT) by a factor  $(\rho_{300\text{K}} - \rho_{2\text{K}})/\rho_{2\text{K}} = 21\%$ . The reference values for the *i*-Au–Al–Yb sample used in [9] are  $\rho_{2\text{K}} = 200 \mu\Omega \text{ cm}$  and  $(\rho_{300\text{K}} - \rho_{2\text{K}})/\rho_{2\text{K}} = 25\%$ . The shape of  $\rho(T)$  of the two samples, showing positive temperature coefficient with a decreasing slope upon heating, is also practically identical. In view of a typical experimental uncertainty of the electrical resistivity due to errors in estimation of the samples' geometrical parameters (the length and the cross section), which is of a few %, the two resistivities can be considered to match well.

Magnetic susceptibility of the *i*-Au–Al–Yb sample was measured in the temperature range 2–380 K in a magnetic field  $H = 1$  kOe. The inverse susceptibility  $\chi^{-1}$  versus temperature is shown in Fig. 2. Solid line is the Curie–Weiss fit  $\chi = C_{\text{CW}}/(T - \theta)$  for temperatures  $T > 100$  K, yielding parameter values  $C_{\text{CW}} = 1.72$  emu K/mol Yb and  $\theta = -148$  K. The Curie–Weiss constant  $C_{\text{CW}}$  was used to determine the mean effective magnetic moment  $\mu_{\text{eff}} = \bar{p}\mu_B$  per Yb atom, where  $\mu_B$  is the Bohr magneton and  $\bar{p}$  is the mean effective Bohr magneton number that can be obtained from the Curie–Weiss constant using formula [11]  $\bar{p} = 2.83\sqrt{C_{\text{CW}}}$ . We obtained  $\mu_{\text{eff}} = 3.71\mu_B$ . Since the ytterbium free-ion Bohr magneton numbers are  $p(\text{Yb}^{3+}) = 4.54$  and  $p(\text{Yb}^{2+}) = 0$ , this confirms the intermediate-valence character of our *i*-Au–Al–Yb sample, in agreement with the samples used in other studies [9,10]. The  $\text{Yb}^{3+}$  fraction was obtained from  $f_{\text{Yb}^{3+}} = (\bar{p}/p(\text{Yb}^{3+}))^2 = 67\%$ , the rest of ytterbium atoms (33%) being in the  $\text{Yb}^{2+}$  state. The reference values for the sample used in [9] are  $\mu_{\text{eff}} = 3.81\mu_B$  and  $\theta = -138$  K, whereas the values for the sample from [10] are  $\mu_{\text{eff}} = 3.91\mu_B$  and  $\theta = -153$  K. The differences in the  $\mu_{\text{eff}}$  and  $\theta$  values of the three samples are small enough to conclude that they are magnetically not significantly different.

Specific heat of our sample was determined between 2 K and RT using a thermal-relaxation calorimeter. The low-temperature specific heat (calculated per mole of  $\text{Au}_{0.51}\text{Al}_{0.34}\text{Yb}_{0.15}$ ) in magnetic fields  $H = 0$  and 90 kOe is shown in Fig. 3 in a  $C/T$  versus  $T^2$  plot, whereas  $C$  as a function of  $T$  in the entire investigated temperature range is shown in the inset. In zero field,  $C/T$  exhibits below 6 K an upturn, which is largely suppressed in the 90 kOe field. Such features are characteristic of exchange-enhanced (interacting-electrons) systems [12], where the low-temperature specific heat is of the type  $C = \gamma T + AT^3 \ln T + \alpha T^3$  with  $\gamma$  and  $\alpha$  being the electronic and lattice specific heat coefficients, respectively, and the  $T^3 \ln T$  term is responsible for the low-temperature upturn. At temperatures above 3 K, the 90 kOe  $C/T$  curve lies above the one in zero field, in agreement with the data of the *i*-Au–Al–Yb sample reported in [9]. (Note that the  $C/T$  values reported in [9] and [10] are given per mole of ytterbium. When recalculated per mole of sample, those values match our values in the investigated

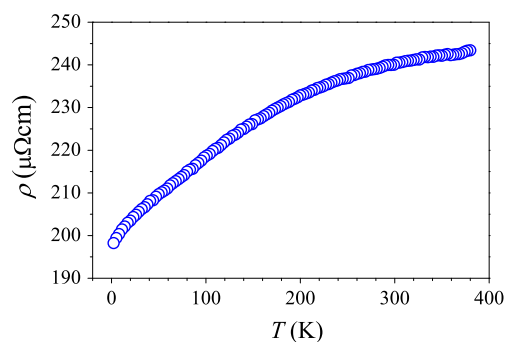
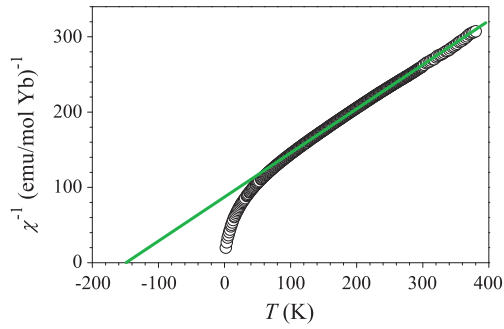
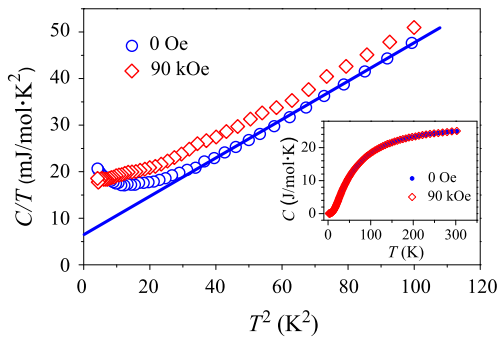


Fig. 1. Temperature-dependent electrical resistivity of the *i*-Au–Al–Yb quasicrystal.



**Fig. 2.** Inverse magnetic susceptibility  $\chi^{-1}$  versus temperature, measured in a magnetic field  $H = 1$  kOe. Solid line is a Curie-Weiss fit  $\chi = C_{CW}/(T - \theta)$  for temperatures  $T > 100$  K.



**Fig. 3.** Low-temperature specific heat in magnetic fields  $H = 0$  and 90 kOe in a  $C/T$  versus  $T^2$  plot. The inset shows  $C$  as a function of  $T$  in the entire investigated temperature range up to room temperature. Solid line is the fit of the zero-field low-temperature  $C/T$  data between 6 and 10 K with the function  $C/T = \gamma + \alpha T^2$ .

temperature range above 2 K.) The specific heat of our sample is thus the same as that of the samples used in other studies [9,10].

As the ytterbium compounds frequently form a heavy-fermion state at low temperatures, it is interesting to check this possibility for the  $i$ -Au–Al–Yb QC by estimating the effective mass  $m^*$  of the conduction electrons relative to the free-electron mass  $m$  from the formula  $m^*/m = \gamma/\gamma_F$ , where  $\gamma_F$  is the free-electron value of the electronic specific heat coefficient. For heavy fermions,  $C/T$  also exhibits an upturn at low temperatures and  $\gamma$  is of the order 100 mJ/mol K<sup>2</sup>, which is by one to two orders of magnitude larger than in exchange-enhanced systems where  $\gamma \sim 10$  mJ/mol K<sup>2</sup>. The free-electron value of the electronic specific heat coefficient can be calculated from the formula [13]  $\gamma_F = 0.136 (A/d)^{2/3} (e/a)^{1/3}$  (in units [mJ/mol K<sup>2</sup>]), where  $A$  is the molar mass in g,  $d$  the density in g/cm<sup>3</sup> and  $e/a$  the number of valence electrons per atom. For the  $Au_{0.51}Al_{0.34}Yb_{0.15}$  composition we take  $A = 135.6$  g,  $e/a = 1.93$  (assuming ionization states Al<sup>3+</sup>, Au<sup>1+</sup>, Yb<sup>3+</sup> for 67% of Yb atoms and Yb<sup>2+</sup> for 33% of Yb atoms), whereas the (unknown) density of  $i$ -Au–Al–Yb was approximated by the density of its 1/1 cubic approximant  $Au_{51}Al_{35}Yb_{14}$  as  $d \approx 4.13$  g/cm<sup>3</sup> (obtained by considering that the approximant's cubic unit cell of edge length  $a = 14.5$  Å contains 89.6 Au + 61.8 Al + 24.0 Yb atoms [1]). The calculation has yielded  $\gamma_F = 1.74$  mJ/mol K<sup>2</sup>. The experimental electronic specific coefficient  $\gamma$  was determined from the fit of the zero-field low-temperature  $C/T$  data between 6 and 10 K with the function  $C/T = \gamma + \alpha T^2$  (solid line in Fig. 3), which yielded  $\gamma = 6.52$  mJ/mol K<sup>2</sup> and  $\alpha = 0.41$  mJ/mol K<sup>4</sup> (wherefrom we obtain the Debye temperature as  $\theta_D = 168$  K). The effective electron mass was then obtained as  $m^* = 3.8m$ , classifying  $i$ -Au–Al–Yb among exchange-enhanced systems, but not as a heavy-fermion compound (where  $m^*$  should be expected in the range from several 10 up to 1000  $m$ ).

### 3. Electronic density of states in the vicinity of Fermi level

In the following we shall present measurements of the temperature-dependent thermoelectric power  $S(T)$  and the Hall coefficient  $R_H(T)$  with the aim to reconstruct the shape of the electronic DOS of  $i$ -Au–Al–Yb in the experimentally observable energy interval of a few  $k_B T$  around the Fermi level  $\epsilon_F$ . We shall demonstrate that the thermopower and the Hall coefficient possess opposite signs,  $S > 0$  and  $R_H < 0$ . Hall coefficient was used to determine the sign of charge carriers, whereas the shape of the DOS was reconstructed from  $S(T)$ .

#### 3.1. Hall coefficient

Measurements of the Hall coefficient were performed by a five-point method using standard ac technique in magnetic fields up to 10 kOe. The current through the samples was in the range 10–50 mA and the measurements were performed in the temperature interval from 90 to 380 K. The experimental uncertainty in  $R_H$  was  $\pm 0.1 \times 10^{-10}$  m<sup>3</sup> C<sup>-1</sup>, which was mainly due to fluctuations of the Ohmic offset caused by silver paint used for the contact preparation. In the investigated temperature interval and for magnetic fields up to 10 kOe, the Hall resistivity  $\rho_H$  was a linear function of the magnetic field, so that we present the results for the Hall coefficient  $R_H$  only. The temperature-dependent  $R_H(T)$  of the  $i$ -Au–Al–Yb sample is presented in Fig. 4a.  $R_H$  is negative and its absolute value decreases with increasing temperature.

In paramagnetic solids with small-enough magnetic susceptibility that the demagnetization fields can be neglected (as is the case for our sample), the Hall effect can be decomposed into the normal Hall effect due to Lorentz force and a strongly temperature-dependent component proportional to magnetization (or magnetic susceptibility  $\chi$ ). The Hall coefficient can be written as [14]

$$R_H = R_0 + \chi R_s, \quad (1)$$

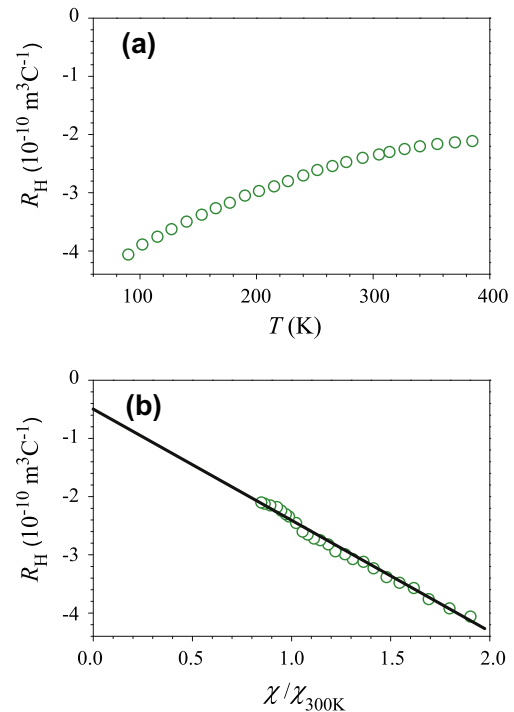


**Fig. 4.** (a) Temperature-dependent Hall coefficient  $R_H(T)$  of the  $i$ -Au–Al–Yb quasicrystal. (b)  $R_H$  as a function of the normalized magnetic susceptibility  $\chi/\chi_{300K}$ . Solid line is the fit with Eq. (1).

where  $R_0$  is the normal Hall coefficient and  $R_s$  is the anomalous Hall coefficient. In Fig. 4b we plot  $R_H$  as a function of  $\chi/\chi_{300K}$ , giving a straight line that confirms the linear relation between  $R_H$  and  $\chi$ . The fit (solid line) was made with the function  $R_H = R_0 + (\chi/\chi_{300K})R_s$ , yielding  $R_0 = -0.5 \times 10^{-10} \text{ m}^3 \text{ C}^{-1}$  and  $R_s = -1.9 \times 10^{-10} \text{ m}^3 \text{ C}^{-1}$ . The normal Hall coefficient  $R_0$  value is typical metallic (with the charge carrier density of the order  $10^{23} \text{ cm}^{-3}$ ) and its negative sign reveals that electrons are the majority charge carriers.

### 3.2. Thermoelectric power

The thermoelectric power (the Seebeck coefficient  $S$ ) of  $i$ -Au–Al–Yb in the temperature interval between 2 and 300 K is shown in Fig. 5a. Upon heating from 2 K,  $S(T)$  is first negative and exhibits a minimum at about 5 K. At 10 K,  $S(T)$  crosses zero (changes sign to positive) and then continuously grows to RT in a nonlinear manner, where it reaches the value  $S_{300K} = 9.1 \text{ } \mu\text{V/K}$ . Theoretical reproduction of this non-trivial  $S(T)$  temperature-dependence will enable us to reconstruction the shape of the spectral conductivity function  $\sigma(\varepsilon)$  in the energy range of a few  $k_B T$  around  $\varepsilon_F$ . Spectral conductivity is related to the electronic DOS  $g(\varepsilon)$  via the Einstein relation  $\sigma(\varepsilon) = (e^2/V) g(\varepsilon)D(\varepsilon)$ , with  $e$  being the charge of the carriers,  $D(\varepsilon)$  is the electronic spectral diffusivity and  $V$  is the sample volume. Under the assumption that energy dependence of the spectral diffusivity can be neglected in the vicinity of Fermi level,  $D(\varepsilon) \approx D(\varepsilon_F)$ , the shape of  $\sigma(\varepsilon)$  is the same as the shape of the DOS function  $g(\varepsilon)$ . In our analysis we shall adopt this approximation.

The thermopower was analyzed by the spectral-conductivity model [15–19], where  $S(T)$  and the electrical conductivity  $\sigma(T)$  (the inverse resistivity  $\sigma = 1/\rho$ ) are both derived from the spectral conductivity  $\sigma(\varepsilon)$ . Using Kubo–Greenwood formalism,  $S(T)$  and  $\sigma(T)$  are given by

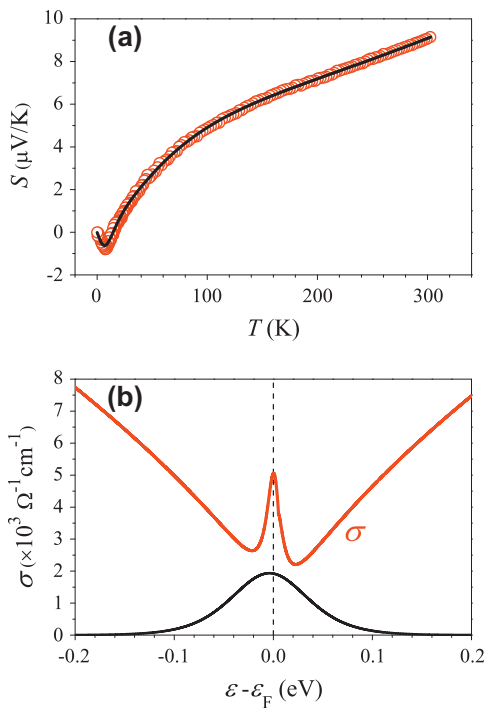


**Fig. 5.** (a) Temperature-dependent thermoelectric power (the Seebeck coefficient  $S$ ) of the  $i$ -Au–Al–Yb quasicrystal. The fit of  $S(T)$  (solid curve) was made with Eq. (2) using the spectral conductivity function  $\sigma(\varepsilon)$  shown in panel (b). (b) Spectral conductivity function  $\sigma(\varepsilon)$  reconstructed from the temperature-dependent thermopower. The experimentally observable part of  $\sigma(\varepsilon)$  is shown, as determined by the width of the thermal observation window  $-\partial f/\partial \varepsilon$ . The bell-shaped function  $-\partial f/\partial \varepsilon$  at 300 K is shown at the bottom (its vertical scale does not conform to the  $\sigma(\varepsilon)$  scale).

$$S(T) = \frac{1}{eT\sigma(T)} \int d\varepsilon \sigma(\varepsilon) (\varepsilon - \mu) \left( -\frac{\partial f}{\partial \varepsilon} \right), \quad (2)$$

and

$$\sigma(T) = \int d\varepsilon \sigma(\varepsilon) \left( -\frac{\partial f}{\partial \varepsilon} \right). \quad (3)$$

Here  $f = \{\exp[(\varepsilon - \mu)/k_B T] + 1\}^{-1}$  is the Fermi–Dirac function and  $\mu$  is the chemical potential, which is written in the low-temperature representation as [20]

$$\mu(T) \approx \varepsilon_F - (k_B T)^2 \frac{\pi^2}{6} \left( \frac{d \ln g(\varepsilon)}{d\varepsilon} \right)_{\varepsilon_F} = \varepsilon_F - \zeta T^2. \quad (4)$$

The only material-dependent quantity in Eqs. (2) and (3) is  $\sigma(\varepsilon)$ , so that proper model of the spectral conductivity function should reproduce  $S(T)$  and  $\sigma(T)$  simultaneously. We note, however, that within the spectral conductivity model, the temperature dependence of  $S$  and  $\sigma$  originates from the Fermi–Dirac function (the temperature-dependent change of width and position of the derivative  $-\partial f/\partial \varepsilon$  on the energy scale, which then probes different portions of the spectral conductivity  $\sigma(\varepsilon)$  at different temperatures) and does not include coupling of electrons to phonons. Any additional temperature dependence of  $S(T)$  and  $\sigma(T)$  originating from the electron–phonon coupling cannot be reproduced by Eqs. (2) and (3). The spectral conductivity model is appropriate for the cases of rapidly varying DOS in the vicinity of  $\varepsilon_F$  and/or weak electron–phonon coupling, where the Fermi–Dirac function yields the dominant contribution to the temperature dependence of the electronic transport coefficients.

Proper modeling of the spectral conductivity  $\sigma(\varepsilon)$ , pertinent to the  $i$ -Au–Al–Yb phase, is a crucial step to reproduce  $S(T)$  in the frame of the above theory. We first note that the experimentally observable part of  $\sigma(\varepsilon)$  is determined by the “thermal observation window”  $-\partial f/\partial \varepsilon$  that is a bell-shaped function centred at the chemical potential  $\mu$  with a temperature-dependent full width at half maximum (FWHM)  $\Delta_f = 3.5 k_B T$ . At  $T = 300 \text{ K}$ ,  $\Delta_f$  amounts to 90 meV, whereas it becomes as small as 3 meV at 10 K. For  $T \rightarrow 0$ ,  $-\partial f/\partial \varepsilon$  becomes a delta function  $\delta(\varepsilon - \varepsilon_F)$ , and Eq. (3) yields the zero-temperature electrical resistivity  $\rho_{T \rightarrow 0} = 1/\sigma(\varepsilon_F)$ . The temperature-dependent chemical potential  $\mu(T) = \varepsilon_F - \zeta T^2$  is shifting the thermal observation window on the energy axis, so that different parts of  $\sigma(\varepsilon)$  contribute to the integrals in Eqs. (2) and (3) at different temperatures. However, the shift of the chemical potential from the Fermi energy is generally small, being at RT typically of the order of a few meV. In modeling  $\sigma(\varepsilon)$ , only its portion in the interval of a few 100 meV around  $\varepsilon_F$  is experimentally relevant for the electronic transport coefficients.

Modelling of  $\sigma(\varepsilon)$  can be realized via many different mathematical functions. Following previous investigations of the thermopower of pseudogap systems  $\text{Al}_{82.6-x}\text{Re}_{17.4}\text{Si}_x$  cubic approximants [21] and icosahedral quasicrystals  $i$ -Al–Cu–Fe [18] and  $i$ -Ag–In–Yb [19], the low-temperature features in  $S(T)$  such as the minimum at 5 K and the sign change at 10 K can only be obtained in cases when  $\sigma(\varepsilon)$  varies rapidly with energy in the immediate vicinity of  $\varepsilon_F$ , i.e., when it exhibits a sharp feature on the energy scale of 10 meV. On this basis we have modeled  $\sigma(\varepsilon)$  by the following trial function that consists of a power-law-type valley and a local maximum (a sharp feature in the form of a Lorentzian) within the valley

$$\sigma(\varepsilon) = A(\varepsilon - \Delta_1)^{2\beta} + \frac{B}{\pi} \frac{\Gamma}{(\varepsilon - \Delta_2)^2 + \Gamma^2}. \quad (5)$$

The valley is determined by the scaling factor  $A$ , the power-law exponent  $2\beta$  and the position  $\Delta_1$  with respect to the Fermi energy (taken to be at the origin of the energy scale;  $\varepsilon_F = 0$ ), whereas the sharp feature is characterized by the height  $B/\pi\Gamma$ , the FWHM  $2\Gamma$

and the position with respect to the Fermi energy  $\Delta_2$ . The set of parameters ( $A, B, \beta, \Gamma, \Delta_1$ , and  $\Delta_2$ ) pertinent to  $\sigma(\varepsilon)$  is then adjusted by fitting the  $S(T)$  data.

The fit of  $S(T)$  obtained with Eq. (2) is presented as a solid curve in Fig. 5a and the corresponding  $\sigma(\varepsilon)$  is shown in Fig. 5b. The fit reproduces excellently the complex temperature dependence of  $S(T)$  in the entire investigated temperature range, including the negative values at temperatures below 10 K with a tiny minimum at 5 K, a sign change to positive at 10 K and a continuously changing slope at higher temperatures. The charge carriers were taken to be electrons (charge  $e = -|e|$ ), in agreement with the negative sign of the normal Hall coefficient. The value of the parameter  $\xi = 0.044 \mu\text{eV}/\text{K}^2$  defined in Eq. (4) yields the shift of the chemical potential from the Fermi energy at the highest measurement temperature of 300 K to be small,  $\mu_{300\text{K}} - \varepsilon_F \approx -4 \text{ meV}$ , with the shift being negative ( $\mu$  shifts below  $\varepsilon_F$ ). In order to obtain converging results, we needed to integrate over an energy interval of  $\pm 10 k_B T$  around  $\varepsilon_F$ , amounting to  $\pm 260 \text{ meV}$  at  $T = 300 \text{ K}$ . Within this energy interval,  $\sigma(\varepsilon)$  exhibits the shape of a power-law-type valley with an additional sharp feature on the scale of 10 meV, where both the minimum of the valley and the sharp feature are located almost at the Fermi level (just a few meV away). The model parameter values of the valley are  $A = 2.2 \times 10^4 \Omega^{-1} \text{ cm}^{-1} \text{ eV}^{-2\beta}$ ,  $2\beta = 0.67$  and the shift from the Fermi energy  $\Delta_1 = 5.2 \text{ meV}$ , whereas the parameters of the sharp feature are  $B = 1.3 \times 10^2 \Omega^{-1} \text{ cm}^{-1} \text{ eV}$ , the FWHM  $2\Gamma = 18.9 \text{ meV}$  and the shift from the Fermi energy  $\Delta_2 = 1.2 \text{ meV}$ . In Fig. 5b, the thermal observation window  $-\partial f/\partial \varepsilon$  at 300 K is shown as well. In order to reproduce the low-temperature features of  $S(T)$ , the presence of a sharp feature at  $\varepsilon_F$  on the scale of 10 meV is essential, as the temperature-dependent chemical potential moves the thermal observation window across the sharp feature on the scale of a few meV, where the slope of  $\sigma(\varepsilon)$  is changing rapidly. The spectral conductivity at  $\varepsilon_F$  amounts to  $\sigma(\varepsilon_F) = 5.0 \times 10^3 \Omega^{-1} \text{ cm}^{-1}$ , yielding the zero-temperature resistivity  $\rho_{T \rightarrow 0} = 1/\sigma(\varepsilon_F) = 200 \mu\Omega \text{ cm}$ , in good agreement with the experimental value  $\rho_{2\text{K}} = 198 \mu\Omega \text{ cm}$  from Fig. 1. Since within the approximation of constant electronic diffusivity in the region close to  $\varepsilon_F$  the energy dependence of  $\sigma(\varepsilon)$  originates from the energy dependence of the electronic DOS  $g(\varepsilon)$ , the shape of  $g(\varepsilon)$  of *i*-Au–Al–Yb (properly scaled) is the same as the shape of  $\sigma(\varepsilon)$  shown in Fig. 5b. We also note that the high sensitivity of  $S(T)$  on the sharp feature in  $\sigma(\varepsilon)$  in the close vicinity of  $\varepsilon_F$  originates from the fact that the thermopower depends on the derivative  $d\sigma(\varepsilon)/d\varepsilon$ . This is best seen by recognizing that the Mott thermopower  $S^M(T) = (\pi^2 k_B^2/3e)(d \ln \sigma(\varepsilon)/d\varepsilon)_{\varepsilon_F} T$  represents the low-temperature limit of the thermopower  $S(T)$  given by Eq. (2) [17]. For rapidly varying derivative  $d\sigma(\varepsilon)/d\varepsilon$  across the sharp feature, the Fermi–Dirac function yields the dominant contribution to the temperature dependence of  $S(T)$ , whereas the possible additional temperature dependence due to electron–phonon coupling is a minor effect, not observed experimentally. In contrast, the electrical conductivity  $\sigma(T)$  given by Eq. (3), being directly proportional to the integral of the spectral conductivity  $\sigma(\varepsilon)$  within the thermal observation window, is less sensitive to the presence of a sharp feature in  $\sigma(\varepsilon)$  on the scale of 10 meV, which does not contribute significantly to the integral. Electron–phonon effects that result in the positive temperature coefficient of the resistivity consequently become more important.

#### 4. Discussion and conclusions

The presented experimental study of the electronic DOS in the region around  $\varepsilon_F$  has revealed that the DOS of the *i*-Au–Al–Yb quasicrystal exhibits a pronounced valley with a sharp feature on the 10 meV scale, both being centered almost exactly at  $\varepsilon_F$ . As

discussed before, the electronic transport coefficients probe the DOS on an energy scale of a few 100 meV around  $\varepsilon_F$  only, and on this local scale, the spectral conductivity function  $\sigma(\varepsilon)$  from Fig. 5b suggests a rather steep pseudogap, which is apparently not wide enough to ensure sufficient electronic energy gain of the order of a few 10 kJ/mol needed for the electronic stabilization of the icosahedral phase. Such large energy gain would require much wider “global” pseudogap with the width in the range 1–2 eV. There exists a realistic possibility that the pseudogap shown in Fig. 5b corresponds to a local valley within fine structure in the DOS on the energy scale of 100 meV in the near Fermi energy region. Fine structure in the DOS on this energy scale was predicted theoretically from first-principles electronic band structure calculations for several quasicrystalline approximants [21–23]. Due to narrow width of the thermal observation window, we are not able to discriminate experimentally between the cases of fine structure within the global pseudogap and in the absence of a global pseudogap. Metastability of the *i*-Au–Al–Yb phase at both low and high temperatures is in favour of the absence of a global pseudogap centred close to  $\varepsilon_F$  that would be wide and deep enough to provide electronic stabilization of the icosahedral phase. A global pseudogap may still be present in the DOS of *i*-Au–Al–Yb, but is perhaps shifted away from the Fermi energy region to the extent that it does not contribute sufficient energy gain for the electronic stabilization of the icosahedral phase. Electronic structure calculations for the 1/1 Ag–In–Yb approximant of Tsai-type QCs have revealed [24] that hybridization of the Yb 5d band with the Ag/In 5p band leads to a dip/pseudogap shifted slightly above the Fermi level, with the Fermi level pinned to the negative-slope side of the pseudogap. Identical situation was also found for another Tsai-type approximant, the Cd<sub>6</sub>Yb [25,26]. A significant shift of the global pseudogap away from the Fermi level could explain metastability of the *i*-Au–Al–Yb QC of composition Au<sub>51</sub>Al<sub>34</sub>Yb<sub>15</sub>. A slight change of composition might shift the Fermi level back toward the center of the pseudogap and provide high-temperature stability of the structure, which could explain the thermodynamic stability of the 1/1 cubic approximant phase of composition Au<sub>51</sub>Al<sub>35</sub>Yb<sub>14</sub>, nearby that of the quasicrystalline phase. First-principles band structure calculations for the approximant are needed to prove/disprove this hypothesis, which may, however, not be easy to conduct due to large amount of chemical and geometrical disorder in the approximant's unit cell originating from mixed and partial occupancies of most lattice sites [1].

The presence of a sharp feature in the DOS at  $\varepsilon_F$  is not uncommon in metallic compounds containing rare earth elements (especially those containing Ce, U and Yb that form heavy-fermion compounds) [27–29]. In such compounds, the *f*-levels lie close to the Fermi level resulting in strong mixing between the conduction electrons and the *f*-electrons. The interaction between these being antiferromagnetic, the conduction electrons may gradually compensate the localized *f*-moment as the temperature is lowered. Simultaneously the overlap of the polarization clouds around the localized moments leads to an indirect interaction between them. The competition between these two effects, coupled with the hybridization of the *f* and *s* states, leads to a sharp resonance peak in the electronic DOS at the Fermi level and hence to an increased electronic specific heat coefficient  $\gamma$  value. The increased  $\gamma$  of the *i*-Au–Al–Yb QC by a factor 3.8 with respect to the free-electron value that is typical of exchange-enhanced systems supports this consideration.

#### Acknowledgment

JJ, PP and AS acknowledge support by the Ministry of Science, Education and Sports of the republic of Croatia through the research Project No. 035-0352826-2848.

## References

- [1] T. Ishimasa, Y. Tanaka, S. Kashimoto, *Philos. Mag.* 91 (2011) 4218.
- [2] A.P. Tsai, J.Q. Guo, E. Abe, H. Takakura, T.J. Sato, *Nature* 408 (2000) 537.
- [3] J.Q. Guo, E. Abe, A.P. Tsai, *Phys. Rev. B* 62 (2000) R14605.
- [4] H. Takakura, C.P. Gómez, A. Yamamoto, M. de Boissieu, A.P. Tsai, *Nat. Mater.* 6 (2007) 58.
- [5] S. Kashimoto, R. Maezawa, Y. Kasano, T. Mitani, T. Ishimasa, *Jpn. J. Appl. Phys.* 42 (2003) L1268.
- [6] R. Maezawa, S. Kashimoto, T. Ishimasa, *Phil. Mag. Lett.* 84 (2004) 215.
- [7] U. Mizutani, *Hume–Rothery Rules for Structurally Complex Alloy Phases*, CRC Press, Taylor & Francis Group, Boca Raton, 2011 (Chapter 2 and Chapter 11).
- [8] U. Mizutani, *Hume–Rothery Rules for Structurally Complex Alloy Phases*, CRC Press, Taylor & Francis Group, Boca Raton, 2011 (Chapter 4).
- [9] T. Watanuki, S. Kashimoto, D. Kawana, T. Yamazaki, A. Machida, Y. Tanaka, T.J. Sato, *Phys. Rev. B* 86 (2012) 094201.
- [10] K. Deguchi, S. Matsukawa, N.K. Sato, T. Hattori, K. Ishida, H. Takakura, T. Ishimasa, *Nat. Mater.* 11 (2012) 1013.
- [11] F.E. Mabbs, D.J. Machin, *Magnetism and Transition Metal Complexes*, Chapman and Hall, London, 1973. p. 7.
- [12] A. Tari, *The Specific Heat of Matter at Low Temperatures*, Imperial College Press, London, 2003. p. 78.
- [13] U. Mizutani, *Introduction to the Electron Theory of Metals*, Cambridge University Press, Cambridge, 2001. pp. 39–42.
- [14] U. Mizutani, *Introduction to the Electron Theory of Metals*, Cambridge University Press, Cambridge, 2001. p. 430.
- [15] C.V. Landauro, H. Solbrig, *Mat. Sci. Eng. A* 294–296 (2000) 600.
- [16] H. Solbrig, C.V. Landauro, *Electronic transport parameters and spectral fine structure*, in: H.-R. Trebin (Ed.), *Quasicrystals, Structure and Physical Properties*, Wiley-VCH, Weinheim, 2003. pp. 254–269.
- [17] C.V. Landauro, H. Solbrig, *Physica B* 301 (2001) 267.
- [18] J. Dolinšek, S. Vrtnik, M. Klanjšek, Z. Jagličič, A. Smontara, I. Simljanić, A. Bilušić, Y. Yokoyama, A. Inoue, C.V. Landauro, *Phys. Rev. B* 76 (2007) 054201.
- [19] M. Bobnar, S. Vrtnik, Z. Jagličič, M. Wencka, Can Cui, An Pang Tsai, J. Dolinšek, *Phys. Rev. B* 84 (2011) 134205.
- [20] N.W. Ashcroft, N.D. Mermin, *Solid State Physics*, Saunders College Publishing, London, 1976. p. 46.
- [21] T. Takeuchi, T. Otagiri, H. Sakagami, T. Kondo, U. Mizutani, H. Sato, *Phys. Rev. B* 70 (2004) 144202.
- [22] U. Mizutani, Y. Kondo, Y. Nishino, M. Inukai, M. Feuerbacher, H. Sato, *J. Phys.: Condens Matter* 22 (2010) 485501.
- [23] N. Wang, W.-Y. Yu, B.-Y. Tang, L.-M. Peng, W.-J. Ding, *J. Phys. D: Appl. Phys.* 41 (2008) 195408.
- [24] H.R. Sharma, G. Simutis, V.R. Dhanak, P.J. Nugent, C. Cui, M. Shimoda, R. McGrath, A.P. Tsai, Y. Ishii, *Phys. Rev. B* 81 (2010) 104205.
- [25] Y. Ishii, T. Fujiwara, *Phys. Rev. Lett.* 87 (2001) 206408.
- [26] Y. Ishii, T. Fujiwara, *J. Alloys Comp.* 342 (2002) 343.
- [27] P. Fulde, *Electron Correlations in Molecules and Solids*, Springer-Verlag, Berlin, 1995.
- [28] S.H. Liu, in: K.A. Gschneidner Jr., L. Eyring, G.H. Lander, G.R. Choppin (Eds.), *Handbook on the Physics and Chemistry of Rare Earths*, vol. 17, Elsevier, 1993 (Chapter 111).
- [29] P. Wachter, in: K.A. Gschneidner Jr., L. Eyring, G.H. Lander, G.R. Choppin (Eds.), *Handbook on the Physics and Chemistry of Rare Earths*, vol. 19, Elsevier, 1994 (Chapter 132).